

Article

Prediction of Potential Evapotranspiration via Machine Learning and Deep Learning for Sustainable Water Management in the Murat River Basin

Ibrahim A. Hasan  and Mehmet Ishak Yuce 

Civil Engineering Department, Gaziantep University, 27410 Gaziantep, Türkiye

* Correspondence: ibrahim.a.blbas@gmail.com (I.A.H.); yuce@gantep.edu.tr (M.I.Y.)

Abstract: Potential evapotranspiration (PET) is a significant factor contributing to water loss in hydrological systems, making it a critical area of research. However, accurately calculating and measuring PET remains challenging due to the limited availability of comprehensive data. This study presents a detailed sustainable model for predicting PET using the Thornthwaite equation, which requires only mean monthly temperature (T_{mean}) and latitude, with calculations performed using R-Studio. A geographic information system (GIS) was employed to interpolate meteorological data, ensuring coverage of all sub-basins within the Murat River basin, the study area. Additionally, Python libraries were utilized to implement artificial intelligence-driven models, incorporating both machine learning and deep learning techniques. The study harnesses the power of artificial intelligence (AI), applying deep learning through a convolutional neural network (CNN) and machine learning techniques, including support vector machine (SVM) and random forest (RF). The results demonstrate promising performance across the models. For CNN, the coefficient of determination (R^2) varied from 96.2 to 98.7%, the mean squared error (MSE) ranged from 0.287 to 0.408, and the root mean squared error (RMSE) was between 0.541 and 0.649. For SVM, the R^2 varied from 94.5 to 95.6%, MSE ranged between 0.981 and 1.013, and RMSE ranged from 0.990 to 1.014. RF showed the best performance, achieving an R^2 of 100%, MSE values of 0.326 and 0.640, and corresponding RMSE values of 0.571 and 0.800. The climate and topography data used for all algorithms were consistent, and the results indicate that the RF model outperforms the others. Consequently, The RF model's superior accuracy highlights its potential as a reliable tool for sustainable PET prediction, supporting informed decision-making in water resource planning. By leveraging GIS, AI, and machine learning, this study enhances PET modeling methodologies, addressing critical water management challenges and promoting sustainable hydrological practices in the face of climate change and resource limitations.

Keywords: PET; sustainable prediction; Thornthwaite equation; CNN; SVM; RF



Citation: Hasan, I.A.; Yuce, M.I. Prediction of Potential Evapotranspiration via Machine Learning and Deep Learning for Sustainable Water Management in the Murat River Basin. *Sustainability* **2024**, *16*, 11077. <https://doi.org/10.3390/su162411077>

Academic Editor: Hossein Bonakdari

Received: 28 November 2024

Revised: 14 December 2024

Accepted: 16 December 2024

Published: 17 December 2024



Copyright: © 2024 by the authors. Licensee MDPI, Basel, Switzerland. This article is an open access article distributed under the terms and conditions of the Creative Commons Attribution (CC BY) license (<https://creativecommons.org/licenses/by/4.0/>).

1. Introduction

Evapotranspiration (ET) describes the process through which moisture is returned from Earth's surface to the atmosphere by combining evaporation from the land and transpiration from plants [1]. In hydrological research, potential evapotranspiration (PET) is widely regarded as a key parameter, essential for validating and refining rainfall-runoff models and broader hydrological cycle assessments, as well as enhancing climate and meteorological forecasting models [2,3]. However, existing PET models often depend on a range of input variables such as temperature, precipitation, solar radiation, wind speed, and humidity, posing challenges when data are sparse or inaccessible [4–7]. This study aims to address these limitations by predicting PET in the Murat River Basin, located in southeast Turkey, using a temperature-only approach. Employing monthly temperature data from the past four decades (1979–2021), we apply the Thornthwaite equation, which requires only temperature and latitude as inputs, making it highly suitable for data-limited environments.

The Murat River Basin is located in the southeastern part of Turkey, which is characterized by a Mediterranean climate, where agricultural water demand is largely driven by ET during the dry season, necessitating extensive irrigation practices in open fields. This challenge is common in semi-arid regions, where limited rainfall necessitates efficient irrigation practices, making accurate PET estimation vital for agricultural planning [4]. The Thornthwaite model has demonstrated robust applicability for PET estimation and aridity assessments across various climatic contexts [8], offering a practical, accessible approach for environments with limited meteorological data.

In response to the predicted impacts of climate change, particularly the Clausius–Clapeyron relationship, which suggests that rising temperature due to climate change will increase atmospheric moisture and intensify the hydrological cycle [9], increasing temperature will enhance the exchange of water vapor between terrestrial ecosystems and the atmosphere. This study explores how PET might respond to these shifts. According to Bouchet’s complementary hypothesis, increased air temperatures could heighten atmospheric evaporative demand, potentially reducing PET rates under specific conditions [10]. Temperature-based PET estimation remains a widely applied and efficient technique in climatology and hydrology, providing an effective means of large-scale modeling [11]. PET plays a crucial role in meteorological research, highlighting the need for reliable measurement methods with guaranteed accuracy in hydrology and agricultural studies [12]. This study presents the sustainability development of a novel PET prediction methodology utilizing Python (google colab version) libraries alongside machine learning and deep learning techniques. Machine learning, in particular, has emerged as an effective tool for forecasting time series data, such as evapotranspiration (ET), independent of prior knowledge of underlying physical processes [3].

There are various methods used to estimate PET in various parts of the world. However, it is a challenge to select a suitable method for PET calculation, because the selection of an appropriate method for certain areas highly depends on data availability [6,7]. As a result of the lack of the required input data in the interested region of study, a key focus of this study is integrating machine learning (ML) and deep learning (DL) methodologies to improve PET predictions. Machine learning models, such as the support vector machine (SVM) [13,14], artificial neural network (ANN) [15], and random forest (RF), have shown promise in enhancing the precision of hydrological forecasting by incorporating complex environmental variables [13,16–18]. SVM, in particular, has demonstrated superior performance in predicting indices like the standardized precipitation index (SPI) when provided with inputs such as wind speed and humidity [15]. Recently, the random forest (RF) method has become more popular because of its robustness and accuracy as a prediction algorithm, despite its simplicity [17,18]. According to Jing et al. (2019), SVM performs optimally when provided with wind speed, rainfall, and relative humidity as inputs. Indeed, deep learning-based models have a remarkable ability to predict future evapotranspiration [16]. Deep learning, through convolutional neural networks (CNNs) and other architectures, has also been successfully applied to time series data, including ET, yielding accurate forecasts in diverse climates [16,19,20].

Despite these advancements, existing PET models frequently lack the flexibility to adapt to varying climatic conditions and often overlook uncertainty factors [19]. This study addresses these gaps by implementing rigorous model validation techniques and uncertainty analyses, providing a robust framework for PET prediction under different climate scenarios. Additionally, we compare traditional approaches with machine learning algorithms to highlight the practical implications of using novel ML and deep learning models in hydrological modeling, particularly its potential for enhancing PET predictions in data-scarce environments. The findings aim to contribute a data-efficient PET prediction methodology, providing a useful tool for regional water management and agricultural planning. This study’s novel approach not only improves upon traditional PET estimation by leveraging artificial intelligence but also seeks to establish a framework that can be adapted to other data-limited regions with similar hydrological needs.

2. Materials and Data Description

2.1. Study Area

The study area is the Murat River Basin in southeastern Turkey, as shown in Figure 1. The Murat River Basin is one of the principal origins of the Euphrates River, which traverses Turkey, Syria, and Iraq in an expansive journey. The latitude and the longitude ranges of the Murat River Basin are $40^{\circ}04'–40^{\circ}02' N$ and $38^{\circ}53'–43^{\circ}46' E$, respectively.

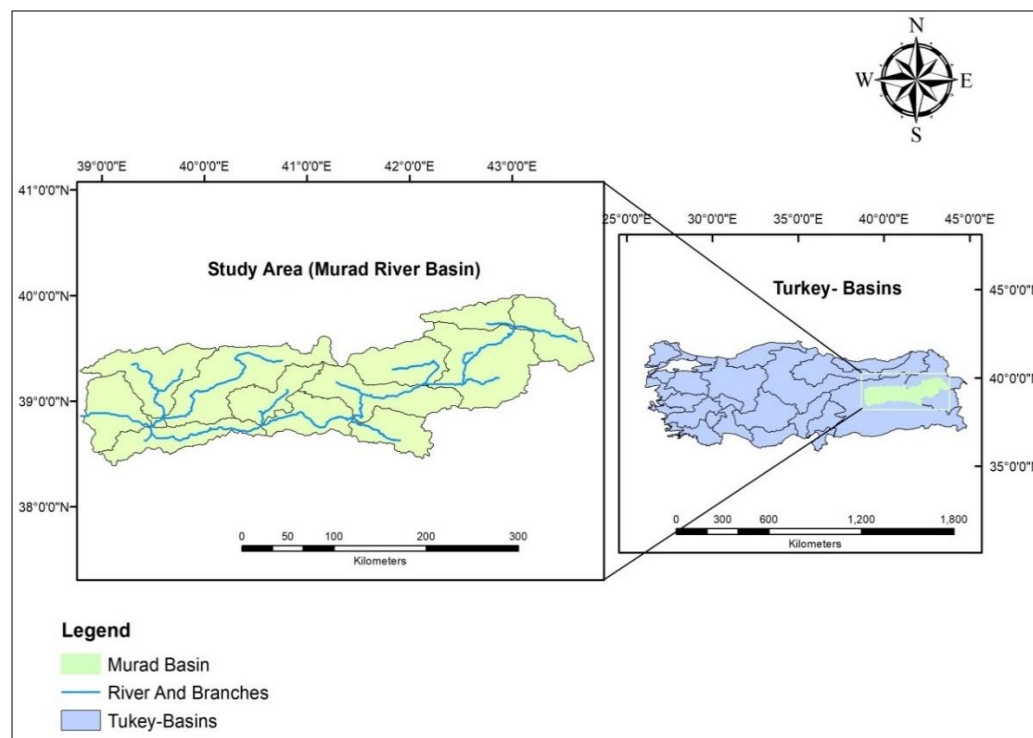


Figure 1. Location of Murat River Basin between Turkey Basins.

The Murat River Basin is characterized by warm–dry summers and cold–wet winters. Precipitation is concentrated during the winter season, from November to April, and the total annual precipitation ranges from 350 to 1010 mm from location to location [21].

2.2. Data Collection

Data collection methods can differ from one country to another, depending on the specific research objectives, data types, units of measurement, and quantity required [22].

In this study, the data include a $12\text{ m} \times 12\text{ m}$ digital elevation model (DEM) sourced from the US Geological Survey (USGS). Mean monthly temperature is the only climate metric used for this study. The data were collected between 1979 and 2021 from 28 meteorological stations around the area, inside and outside the Murat River Basin. Table 1 lists the meteorological stations with their coordinates and serial numbers. This dataset is sufficient for conducting a comprehensive analysis and evaluation within this research area.

Table 1. List of meteorological stations inside and outside the Murat River Basin.

SN	Station Name	Latitude	Longitude
17,099	Ağrı	39.7253	43.0522
17,720	Doğubeyazıt	39.5396	44.018
17,203	Bingöl	38.8847	40.5007

Table 1. *Cont.*

SN	Station Name	Latitude	Longitude
17,776	Solhan	38.9597	41.0503
17,808	Genç	38.7477	40.5528
18,176	Kığı	39.3086	40.3458
17,205	Tatvan	38.5033	42.2808
17,208	Bitlis	38.475	42.1625
17,810	Ahlat	38.7487	42.475
17,094	Erzincan	39.7523	39.4868
17,718	Tezcan	39.7769	40.3906
17,096	Erzurum Havalimanı	39.9529	41.1897
17,666	İspir	40.4861	40.9996
17,668	Oltu	40.5497	41.9951
17,688	Tortum	40.3013	41.5409
17,690	Horasan	40.0415	42.173
17,740	Hınıs	39.3688	41.6957
17,100	Iğdır	39.9227	44.0523
17,097	Kars	40.6061	43.1119
17,656	Arpaçay	40.8431	43.3278
17,692	Sarıkamış	40.3329	42.5983
17,204	Muş	38.7509	41.5023
17,734	Divriği	39.3618	38.1142
17,762	Kangal	39.2428	37.389
17,172	Van Bölge	38.4693	43.346
17,784	Erciş	39.0198	43.3386
17,812	Özalp	38.6573	43.9767
17,852	Gevaş	38.2963	43.1197
17,880	Başkale	38.0435	44.0173

3. Methodology

The methodology adopts a systematic approach, integrating various techniques to guide the workflow of the calculation and prediction of PET by various deep and machine learning algorithms based on temperature data in the study area (Figure 2).

3.1. Geographic Information System (GIS) Spatial Analysis and Modeling Setup

This study geographically analyzes and models the Murat River Basin, with a primary focus on predicting PET. The analysis begins by utilizing ArcGIS software (version 10.8) to extract a high-resolution DEM with a spatial resolution of 12 m × 12 m. This detailed DEM allows for an accurate calculation of the basin's total area, which is approximately 40,000 km². Understanding the basin's dimensions and topography is essential for effective hydrological modeling and predicting PET, as these factors significantly influence water movement and availability within the region.

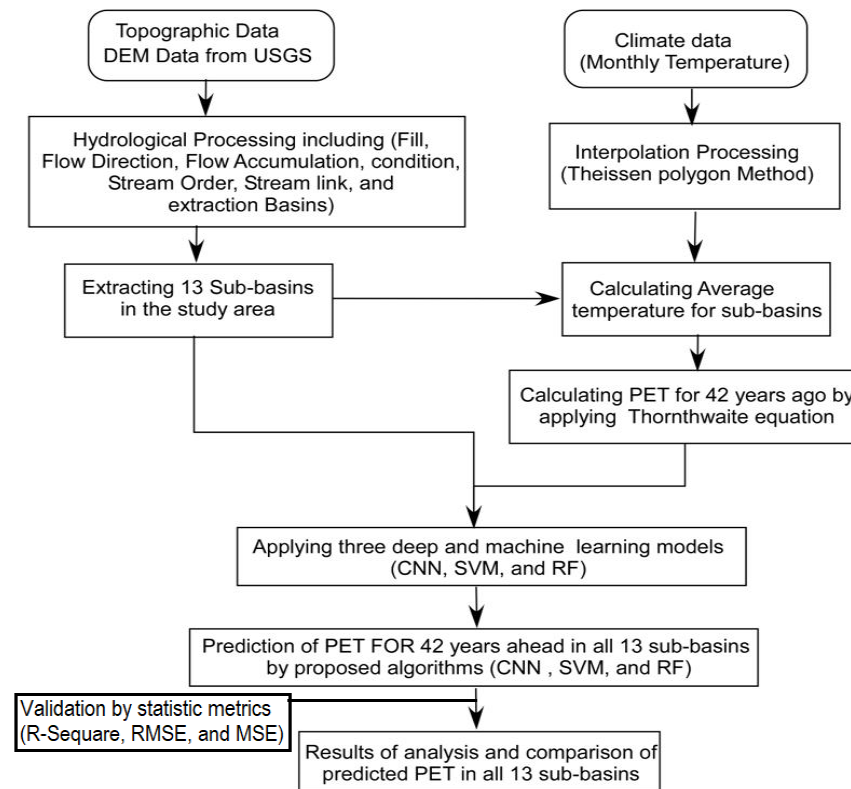


Figure 2. The flowchart depicts the methodological steps of this study.

Thirteen distinct sub-basins were delineated through a comprehensive investigation of various hydrological processes, including filling, flow direction, flow accumulation, stream order, stream link, and basin analysis using GIS. This systematic approach enhances our understanding of the hydrological characteristics of the Murat River Basin, as illustrated in Figure 3. By identifying these sub-basins, we can better assess the spatial variability of hydrological phenomena, which is critical for accurate predictions of PET and effective water resource management in the region.

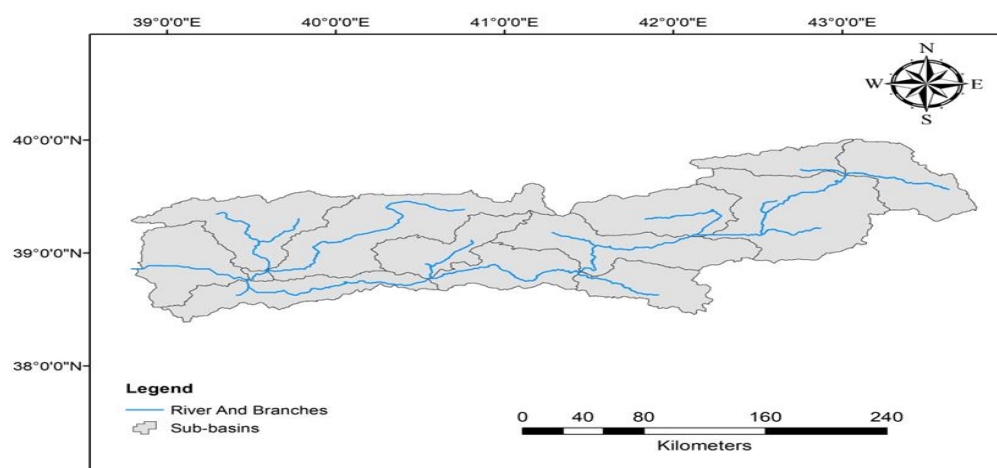


Figure 3. Sub-basins of the Murat River Basin extracted by Arc-Map version 10.8.

3.2. Interpolation Process Using the Thiessen Polygon Method

We employed the Thiessen polygon method for spatial interpolation in ArcGIS, creating polygons around each meteorological station based on its proximity to neighboring stations. This technique allows for a spatial representation of the catchment zones within the basin. The method operates under the assumption that the temperature recorded

at each meteorological station serves as the best estimate for that station's surrounding area compared to any other station's measurements [23]. This approach is particularly useful for capturing the spatial variability of temperature across the Murat River Basin, which is essential for accurate predictions of PET and for understanding the region's hydrological dynamics.

Figure 4 illustrates that meteorological data were collected over at least 40 years from 28 stations located both within and outside the research area. The geographical coordinates of these stations were integrated into the DEM to determine their relative distances and influence on the nearest sub-basins. Spatial interpolation methods are widely utilized to estimate meteorological data values in areas lacking direct measurements [24].

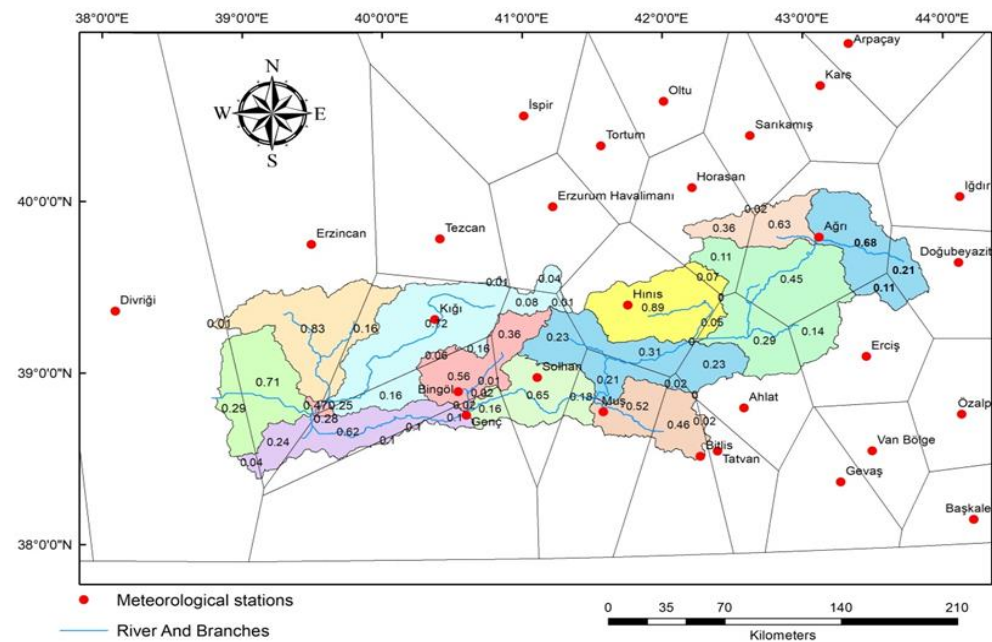


Figure 4. Thiessen polygon method applied to meteorological stations in the Murat Basin.

In this analysis, a weighted temperature value was computed for each station, calculated as the area influenced by the station divided by the total area of the respective sub-basin. This method allows us to assess the temperature contribution of individual stations within each sub-basin, as detailed in Table 2. The resulting data are then integrated to estimate temperature variations across the entire sub-basin, providing a comprehensive understanding of the thermal dynamics within the Murat River Basin.

Table 2. Effective weight of the meteorological stations in the sub-basins.

Sub-Basins	Area	Eff. Weight	Met. Stations
Sub-Basin 1	2957	0.68	AĞRI
		0.11	ERCIŞ
		0.21	DOĞUBEYAZIT
Sub-Basin 2	1601	0.63	AĞRI
		0.37	HORASAN
Sub-Basin 3	5989	0.45	AĞRI
		0.14	ERCIŞ
		0.11	HORASAN
		0.3	AHLAT
Sub-Basin 4	3176	0.88	HINIS
		0.07	HORASAN
		0.05	AHLAT

Table 2. Cont.

Sub-Basins	Area	Eff. Weight	Met. Stations
Sub-Basin 5	4047	0.32	HINIS
		0.22	MUŞ
		0.23	AHLAT
		0.23	SOLHAN
Sub-Basin 6	2259	0.53	MUŞ
		0.47	BITLIS
Sub-Basin 7	2437	0.18	MUŞ
		0.65	SOLHAN
		0.17	GENÇ
Sub-Basin 8	2320	0.36	SOLHAN
		0.08	KIĞI
		0.56	BİNGÖL
Sub-Basin 9	5836	0.1	SOLHAN
		0.73	KIĞI
		0.17	BİNGÖL
Sub-Basin 10	2839	0.1	GENÇ
		0.64	BİNGÖL
		0.26	ERZICAN
Sub-Basin 11	4039	0.84	ERZICAN
		0.16	KIĞI
Sub-Basin 12	137	0.28	BİNGÖL
		0.47	ERZICAN
		0.25	KIĞI
Sub-Basin 13	3058	0.29	DIVRIĞI
		0.71	ERZICAN

3.3. Computing Potential Evapotranspiration (PET)

The Thornthwaite equation is used to calculate potential evapotranspiration (PET) based on temperature and latitude [25]. It can be expressed mathematically as follows:

$$E_T = 1.6 L_a \left[\frac{10 \bar{T}}{I_t} \right]^a, \quad (1)$$

where, E_T is monthly PET (cm); L_a is adjustment for the number of daylight hours and days in the month (depending on latitude; \bar{T} denotes mean monthly air temperature ($^{\circ}\text{C}$); I_t presents the total 12 m monthly values of the heat index, i

$$i = \sum_1^{12} i \quad (2)$$

$$\text{and } i = \left(\frac{\bar{T}}{5} \right)^{1.514} \quad (3)$$

a is empirical constant, where

$$a = 6.75 \times 10^{-7} (I_t)^3 - 7.71 \times 10^{-5} (I_t)^2 + 1.792 \times 10^{-2} (I_t) + 0.49239. \quad (4)$$

The Thornthwaite equation was sustainably implemented using R-Studio (version 2023.03.1+446) to calculate PET. Additionally, standardized precipitation evapotranspiration index (SPEI) values for a long-term series related to the Murat River Basin were generated using R. The Thornthwaite equation calculated the monthly PET. The temperature-derived data were then used to calculate various PET timeframes [26].

3.4. Machine Learning and Deep Learning

In recent years, machine learning and deep learning techniques have significantly advanced the field of climate data analysis and prediction [27]. After computing the potential evapotranspiration (PET) for the past 42 years using temperature data and the Thornthwaite equation, three different machine learning models will be employed to predict PET for the succeeding 42 years. These models will utilize historical temperature data and PET values to identify patterns and relationships that can be applied to future projections. The selected machine learning and deep learning algorithms will be chosen for their capacity to capture nonlinear patterns, temporal dependencies, and complex interactions between temperature and PET. By applying these advanced techniques, this study aims to generate more accurate and reliable forecasts of PET, providing valuable insights into potential future changes in evapotranspiration patterns. The outcomes of these predictions will be essential for understanding long-term evapotranspiration trends and their impact on regional hydrological processes and water resource management. This section explores the utilization of SVM, RF, and CNN to predict PET using temperature data spanning the last forty years. PET is an essential component of hydrological studies, relating temperature to the potential evaporation rate. Given the complex, nonlinear nature of climate data, these advanced algorithms are employed to uncover patterns and improve prediction accuracy.

The dataset was divided into an 80% training set and a 20% testing set to rigorously evaluate each model's performance. All algorithms were implemented using Python libraries, and their outcomes were compared to determine their efficacy in PET prediction. The SVM model is known for its robustness in high-dimensional spaces and performs well in classification tasks, though it may require careful tuning to manage its false positive rates. RF, an ensemble learning method, combines multiple decision trees to enhance predictive accuracy and mitigate overfitting, making it a promising candidate for this study. CNNs are typically used in image recognition tasks and were adapted here to capture the temporal and spatial dependencies in the climate data, leveraging their deep learning capabilities to model complex interactions [28–30]. In terms of comparison, CNN, SVM, and RF models each provide distinct advantages in predicting PET. CNNs are particularly effective at capturing spatial and temporal dependencies, modeling nonlinear relationships, and processing high-dimensional data without the need for manual feature engineering [31]. However, their application requires substantial computational resources and large datasets [20,31]. SVMs, known for their accuracy with structured data, are resistant to overfitting and utilize kernel functions to map data into higher-dimensional spaces. Nonetheless, they are sensitive to hyperparameter tuning and are less scalable for large datasets [32,33]. RF, as an ensemble method, demonstrates robustness to noise and missing data, offers interpretable feature importance, and is computationally efficient, though it is less suited for capturing complex spatial–temporal patterns. By integrating the complementary strengths of these algorithms, this study enhances the accuracy and reliability of PET predictions, providing valuable insights into evapotranspiration trends [31,33,34].

3.4.1. Convolutional Neural Network (CNN)

A CNN is a deep learning algorithm specifically designed to analyze structured grid data, such as images or spatial datasets. It excels in tasks such as pattern recognition, feature extraction, regression, and classification. By employing convolutional layers, CNNs automatically learn spatial feature hierarchies from input data through localized networks. This construction makes them predominantly effective for managing complex and large datasets [20]. According to our performance assessment measures, the CNN technique was suitable for accurately modeling monthly PET. Furthermore, the CNN framework fared better than the artificial intelligence (AI) method in assessing the same locations with the same data inputs. The results of the literature based on the different performance criteria demonstrate that the suggested CNN model can effectively forecast perspective ET because

it can capture the high nonlinearity of evaporation [16,30]. The CNN model's performance is demonstrated in predicting PET across thirteen sub-basins.

3.4.2. Support Vector Machine (SVM)

SVM is a data-driven method in applied mathematics and learning theory that can solve problems via classification and regression [33–35]. SVM employs a hyperplane to split data from one dimension to a high-dimensional space and then solves the regression issues using the following equation:

$$y = f(x) = \sum_{i=1}^n w \times k(x_i, x) + b, (x), \quad (5)$$

where $k(x_1, x)$ is the kernel function, w is the weight vector, and b is the value. By minimizing the total of the squared deviations, the least squares method can calculate the values of the internal parameters. The relation between the actual and predicted PET curve performance of the 13 models was calculated using SVM. The minimal dispersion between the training and testing points indicates a high level of model accuracy and robustness. SVM regression is a supervised machine learning approach used for regression tasks that aims to approximate the relationship between input and output variables. SVM uses kernel functions (e.g., linear, polynomial, or radial basis functions) to transform data into a higher-dimensional space and then determines a hyperplane that fits the input within a specified tolerance. It seeks to minimize errors while remaining simple, defining the margin with support vectors. SVM is particularly successful for high-dimensional and nonlinear data, is resistant to overfitting, and provides flexibility through a variety of kernel options [15,35]. It is commonly used in predictive modeling, time series forecasting, environmental modeling, and signal processing, and its performance is improved by hyperparameter optimization, which is often accomplished using methods such as grid search [15].

3.4.3. Random Forest (RF)

RF has been used to estimate reference evapotranspiration (ET_o) in numerous studies [32,36,37]. However, it does not seem to have been applied to estimating crop evapotranspiration (ET_c) in any previous research.

RF is a supervised ensemble machine learning model used to solve both regression and classification issues. In the real world, forests are made up of multiple decision trees, with the strength of the forest increasing with the number of trees [32,36,38]. Likewise, the RF method generates separate decision trees by randomly selecting a training sample. Random forest regression is an effective machine learning approach that integrates predictions from many decision trees to improve accuracy and eliminate variation. It effectively handles nonlinear relationships, outliers, and missing data while also providing feature importance for data interpretation. While computer-intensive, costly, and less interpretable than simpler models, it is frequently employed in environmental science, geology, and water management for weather forecasting and hydrological estimation. Tuning hyperparameters improves performance, making it a useful tool for complex, high-dimensional datasets [36].

3.5. Models' Performance Validation

This study will delve into the detailed performance of these models, highlighting the variations in their predictive capabilities. The analysis will include statistics metrics such as R^2 , mean squared error (MSE), and root mean squared error (RMSE). Scatterplot matrices will be used to visualize the relationships between actual and predicted PET values, and learning curves will illustrate the models' training progress and convergences. By comparing these advanced algorithms, this section will identify the most effective methods for accurately predicting PET, contributing to improved water resource management and agricultural planning in the context of climate variability.

R-squared, also known as the coefficient of determination, is a statistical metric that represents the proportion of variance in the dependent variable (\hat{y}) that is accounted for

by the independent variable(s) in a regression model. Its value ranges from 0 to 1, where higher values indicate a better fit of the model to the data. R^2 is computed by Equation (6) as follows:

$$R^2 = 1 - \frac{xx_{\text{res}}}{xx_{\text{tot}}} \quad (6)$$

where xx_{res} denotes the error in predictions by measuring the deviation between predicted and observed values, and xx_{tot} indicates the total variability present in the observed values, representing the extent of dispersion or spread within the dataset.

The mean squared error (MSE) is a statistical measure that quantifies the average squared difference between observed and predicted values in a dataset. It is widely utilized in regression analysis, machine learning, and forecasting to evaluate the accuracy of predictive models, with smaller MSE values indicating better model performance.

$$\text{MSE} = \frac{1}{n} \sum_{i=1}^n (y - \hat{y})^2 \quad (7)$$

where y represents observed values, \hat{y} is predicted values, and n is the total number of observations.

The root mean squared error (RMSE) is a widely used metric for assessing the accuracy of predictive models. It quantifies the average magnitude of the difference between estimated and observed values, expressed in the same units as the target variable [28]. RMSE is calculated as the square root of the mean squared error (MSE), providing an interpretable measure of the model error directly comparable to the scale of the data.

$$\text{RMSE} = \sqrt{\text{MSE}} \quad (8)$$

4. Results and Discussion

4.1. PET Calculated with the Thornthwaite Equation

R-Studio was used to calculate PET with the Thornthwaite equation. The input variables were the temperature and latitude of the Murat Basin, located between 39° N and 43° N in the universal transverse mercator (UTM) system. The process was conducted for all 13 sub-basins, with detailed results provided as Supplementary Materials in the form of Excel sheets (refer to the files labeled as “PET Results of Thornthwaite Equation”). From the results, a distinct seasonal pattern emerges. During the colder months (January and February), the average temperatures (T_{avg}) are significantly low, leading to zero or very low PET values across all sub-basins. For instance, in January 1979, the T_{avg} in Sub-basin 4 was -4.69 °C, resulting in a PET of 0.00 mm. Similarly, in February of the same year, Sub-basin 4 maintained a T_{avg} of -1.57 °C, with a corresponding PET of 0.00 mm.

As temperatures rise in the spring and summer months (April to August), PET values increase substantially. For example, in May 1979, Sub-basin 4 recorded a T_{avg} of 11.60 °C, resulting in a PET of 66.88 mm, which is a stark contrast to the values observed in January. This trend was further amplified in July 2016, when Sub-basin 4 recorded a T_{avg} of 21.26 °C with a PET of 133.07 mm, indicating the strong influence of temperature on PET during warmer months. The analysis of the relationship between average temperature (T_{avg}) and potential evapotranspiration (PET) across all sub-basins demonstrates a strong positive correlation, aligning with the principles of the Thornthwaite equation. PET values are negligible or zero when T_{avg} falls below 0 °C, predominantly during the winter months, indicating minimal evaporation potential under cold conditions. As temperatures rise above 0 °C in spring, PET begins to increase, with a more pronounced escalation during summer, when T_{avg} reaches its annual peak.

Across all sub-basins, PET exhibits a consistent upward trend with increasing T_{avg} , peaking during the summer months (e.g., July and August). However, inter-sub-basin variations point to the influence of local climatic and topographical factors: higher-elevation sub-basins show delayed PET responses due to cooler temperatures, whereas lower-elevation or warmer regions display elevated PET peaks. These findings underscore the high sensitivity

of PET to temperature fluctuations and reveal the significant influence of seasonal trends on evapotranspiration-driven water loss. This emphasizes the pivotal role of temperature in regulating evapotranspiration rates and highlights the potential implications of climate variability for regional water resource management.

Figure 5 shows the average monthly PET across 13 sub-basins, derived using the Thornthwaite equation and long-term temperature data spanning 1979 to 2021. The analysis reveals distinct seasonal trends, with PET values peaking during the summer months (June, July, and August) and reaching their lowest in the winter months (December, January, and February) due to average temperature variation. Notably, July records the highest PET values across all sub-basins, exceeding 120 mm, while January exhibits the lowest PET values, falling below 20 mm. Although the general seasonal PET pattern is parallel and consistent, variations in PET values among the sub-basins are noticeable and apparent, the result of being influenced by variances in terrain, altitude, and localized climatic circumstances. For example, Sub-basin 5 exhibits slightly reduced PET values during the summer compared to other sub-basins, signifying that higher altitude or cooler local temperatures may mitigate PET in this area. Conversely, Sub-basin 9 demonstrates higher values of PET in both summer and transitional months (May and September), possibly indicating comparatively warmer conditions or lower humidity levels that enhance evaporation rates. Transitional months, such as April and October, also show noticeable variability. Sub-basin 13, for instance, experiences a significant increase in PET in April relative to other sub-basins, representing an earlier beginning of warmer conditions in the region. Likewise, Sub-basin 3 reveals an obvious decline in PET during October, which may mirror former cooling trends or exact microclimatic factors reducing PET during autumn. These findings underscore the heterogeneity of PET dynamics within the area, caused by localized factors such as altitude gradients, microclimatic conditions, and vegetation cover effects. Such sub-basin-specific variations are crucial for effective agricultural planning and water resource management, as they highlight the extent of the potential severe water stress or demand during specific times of the year. For example, sub-basins with constantly high PET values, such as Sub-basin 9, may involve more concentrated irrigation strategies during peak months, whereas zones with lower PET values, such as Sub-basin 5, might certainly experience reduced water stresses. The sub-basin-level detail provided by this PET analysis offers a valuable understanding of sustainable water resource management. It emphasizes the essential to account for spatial variability in climate-driven factors when scheming irrigation systems, approximating water accessibility, and preparing climate adaptation actions within the region.

4.2. PET Prediction via CNN

The findings reveal a strong correlation between observed and predicted PET values across most sub-basins, underscoring the CNN model's effectiveness in estimating PET. In the graphical outputs, red lines represent predicted values, while blue points depict observed measurements; ideally, these points align closely with the red line, indicating high predictive accuracy. Sub-basins 1, 5, 8, and 10 display a clear linear relationship, with predicted values closely mirroring observed data. In contrast, Sub-basins 3 and 12 contain some outliers, suggesting that minor adjustments to model calibration may enhance accuracy. Notably, Sub-basins 6 and 7 show more pronounced deviations, indicating possible inconsistencies that merit further investigation into factors affecting evaporation in these regions. Overall, the model performs robustly across the majority of sub-basins, suggesting a strong capacity to generalize across diverse geographic and climatic conditions (Figure 6). Although the CNN model demonstrates considerable promise for predicting potential evaporation, addressing the identified outliers will further improve its predictive accuracy. Future model enhancements, such as hyperparameter tuning and integrating additional data sources, could also improve performance in more variable regions.

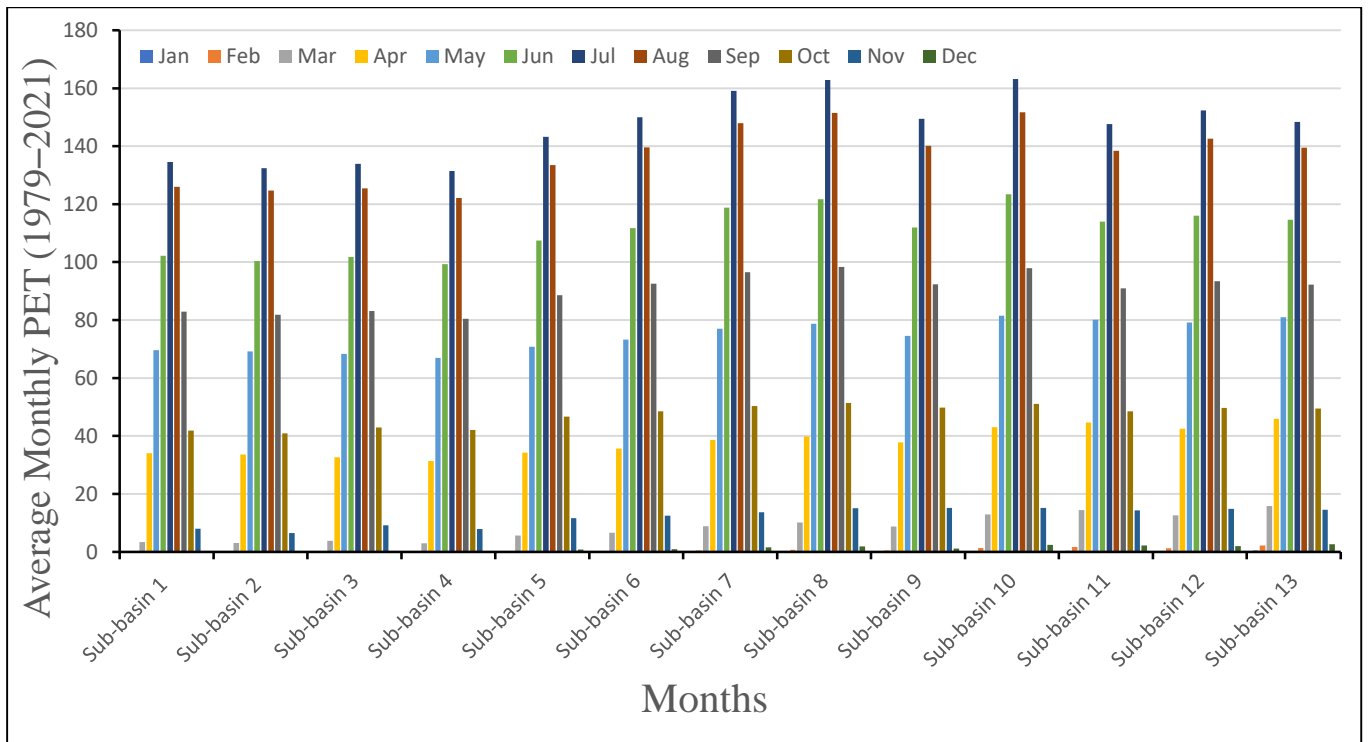


Figure 5. Average monthly PET calculated with Thornthwaite equation (1979–2021).

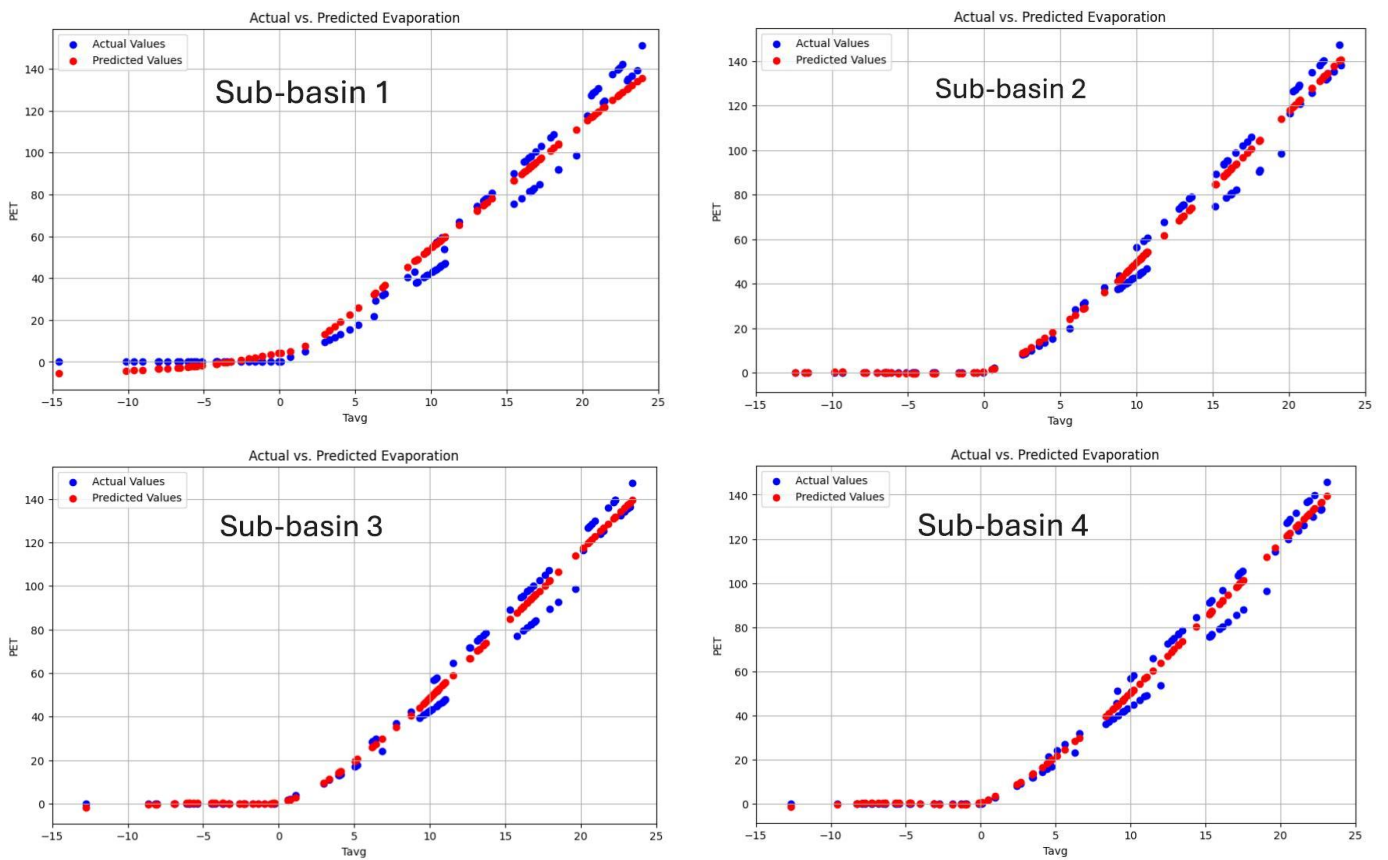


Figure 6. Cont.

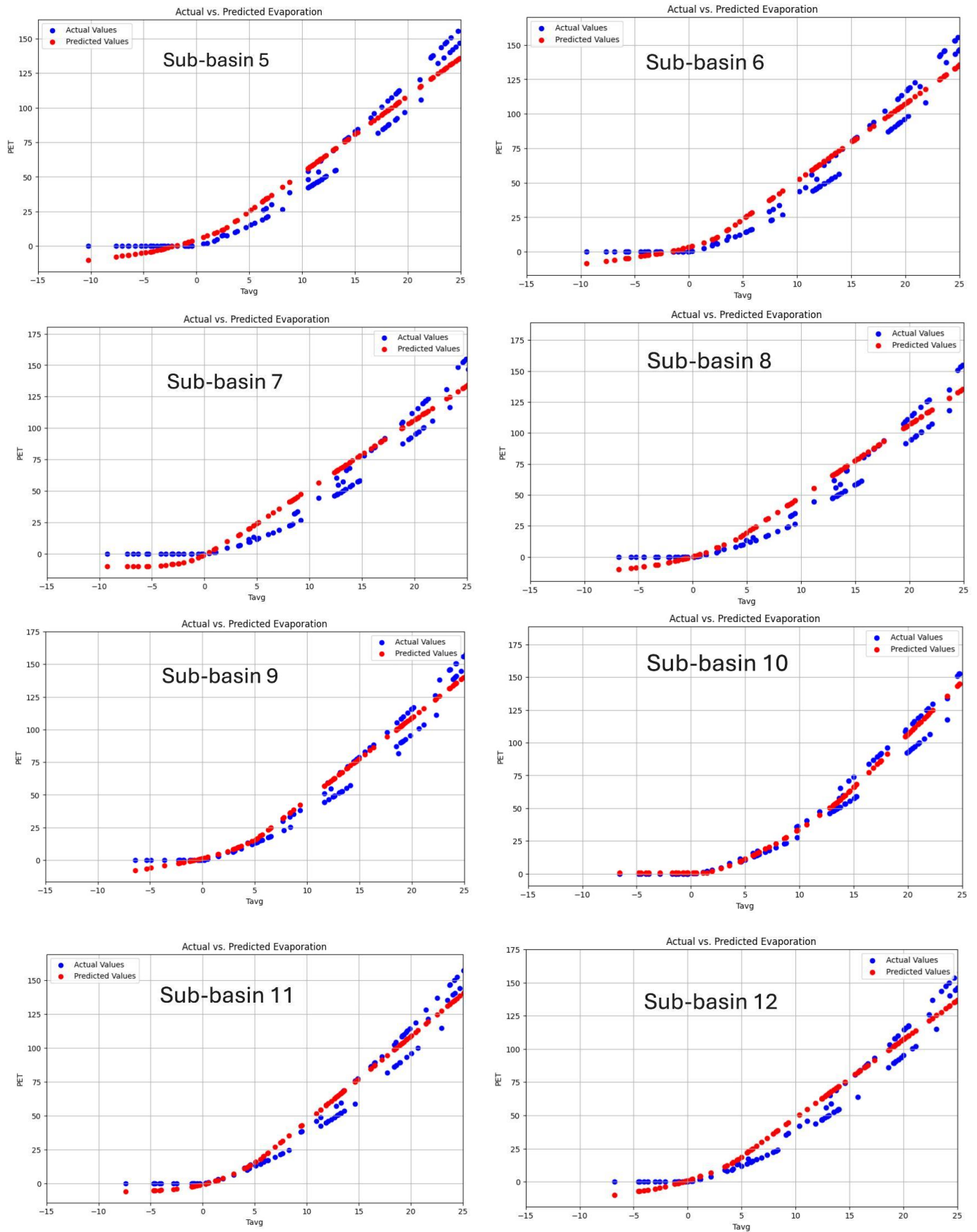


Figure 6. Cont.

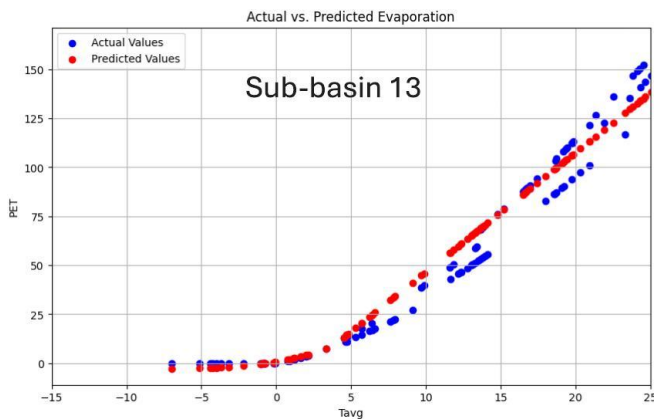


Figure 6. Actual and predicted PET calculated via CNN.

4.3. PET Prediction via SVM

The SVM model demonstrates robust and reliable performance across all sub-basins, with metrics indicating high R^2 and low MSE AND RMSE, underscoring its suitability for predictive tasks in diverse sub-regional contexts, which is parallel to previous studies [30,38,39].

The results provide a comparative analysis of actual and predicted PET across 13 sub-basins, modeled using an SVM. Each sub-basin is represented by a graph that plots PET against temperature (denoted as “Temp”, likely in degrees Celsius). Blue dots indicate the observed recorded PET values, while a red dashed line illustrates the PET values predicted by the SVM model. In each plot, predicted values (blue dots) are displayed alongside observed values (red dots), and the alignment of these points demonstrates a strong correlation between predictions and observations. This close alignment reflects the model’s high accuracy in estimating PET. Across all sub-basins, a positive correlation between temperature and PET is evident; as temperature rises, so does PET (Figure 7). This trend aligns with expectations, as higher temperatures generally increase evaporation and plant transpiration.

The SVM model appears to perform reasonably well in most sub-basins, as the red prediction line generally follows the trend of the actual PET data. However, predictive accuracy varies among sub-basins. In some cases, the predicted line closely matches the real values, indicating a strong fit, while in others, noticeable deviations particularly at higher temperatures propose slight overestimations or underestimations by the model. Certain sub-basins, such as 1, 2, and 3, exhibit a more linear relationship between temperature and PET, while others, including Sub-basins 7 and 10, display a more curvilinear pattern. This variation may reflect differing local environmental factors, such as vegetation cover, soil type, and water availability, which can affect PET behavior. Notably, Sub-basin 12 demonstrates lower PET values across the temperature range in comparison to other sub-basins, suggesting unique characteristics influencing PET in this area.

The graphic advocates that the projected and observed PET values by the SVM model are effective for PET estimation across diverse hydrological settings, each with unique environmental conditions, highlighting its potential applications in water resource management and hydrological modeling [40,41].

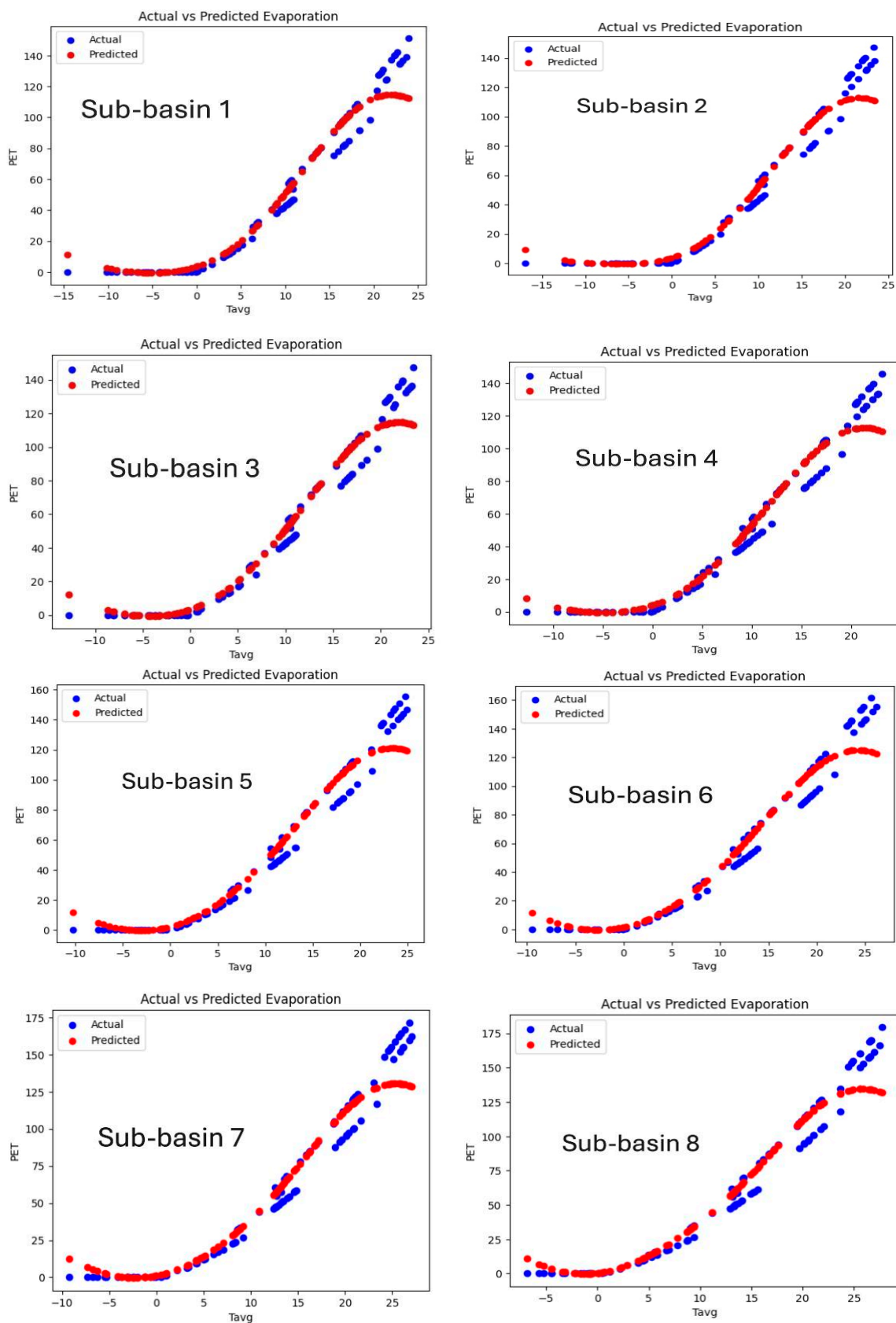


Figure 7. Cont.

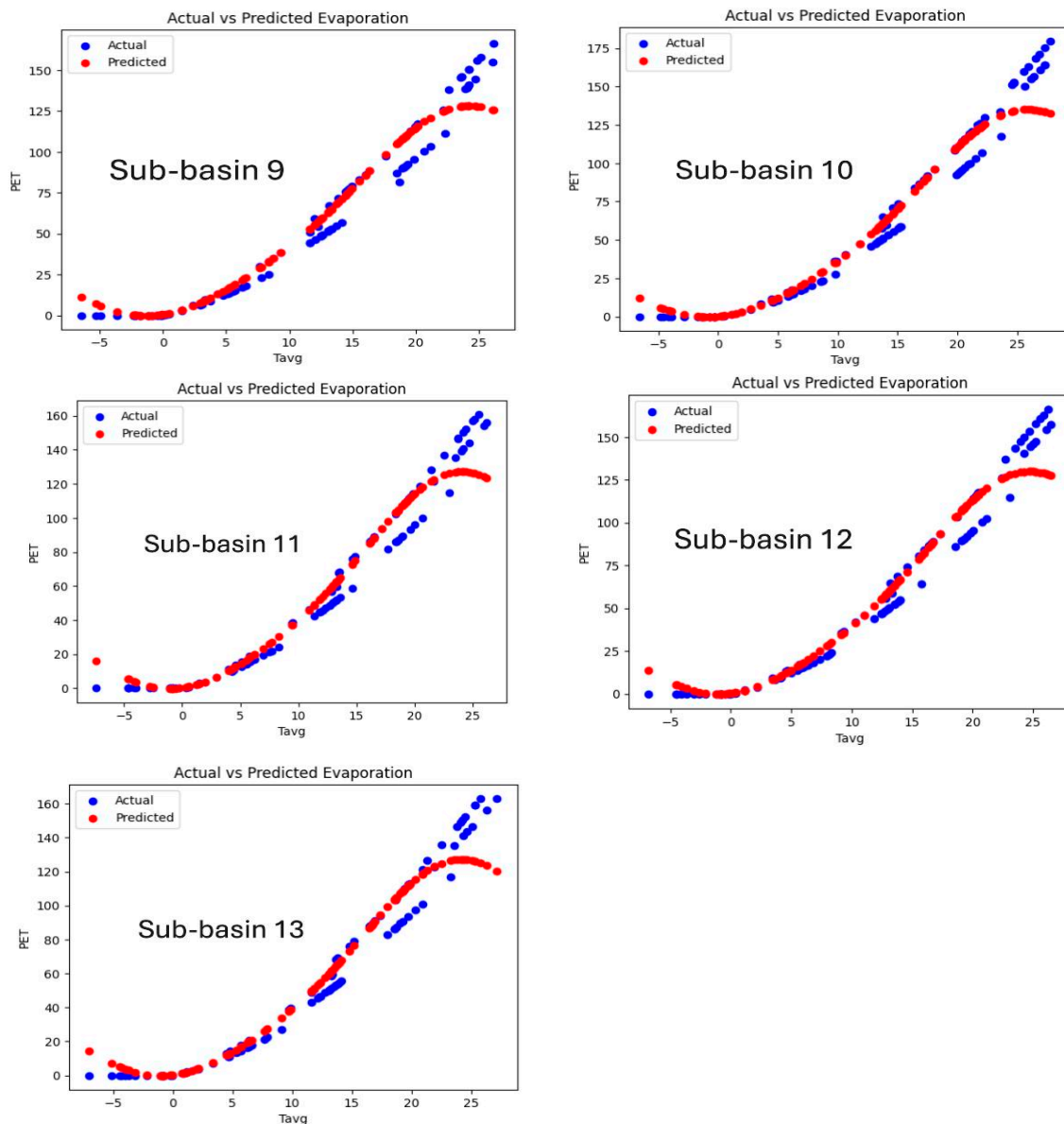


Figure 7. Predicted and actual PET via SVM.

4.4. PET Prediction via RF

After obtaining predictions from each decision tree, the final results for the regression problem were determined by averaging the outputs of all trees. For the classification problem, the final result was derived from a majority vote among all trees. The RF model can overcome the high-dimensional data and strong nonlinear problems, reducing the overfitting by averaging the results [38]. The results demonstrate the RF model's superiority in this context, making it a highly suitable choice for accurate and dependable PET predictions across diverse sub-basins.

Figure 8 demonstrates an evaluation of an RF model's predictions of PET across 13 sub-basins by comparing observed measured data and predicted values. Each of the 13 plates corresponds to a specific sub-basin. Each subplot represents the model's performance, with points aligned along the diagonal 1:1 line indicating accurate predictions. The results reveal strong predictive performance across most sub-basins, with minimal deviations, particularly in low and mid-range PET values. However, slight underestimations are observed at higher PET values in sub-basins such as 7, 8, and 10. Sub-basins 3, 5, and 12 exhibit tightly clustered points along the diagonal, demonstrating robust accuracy,

while Sub-basins 2 and 6 show minor scatter, suggesting some variability in predictions. These observations highlight the model's general effectiveness while indicating areas for potential refinement.

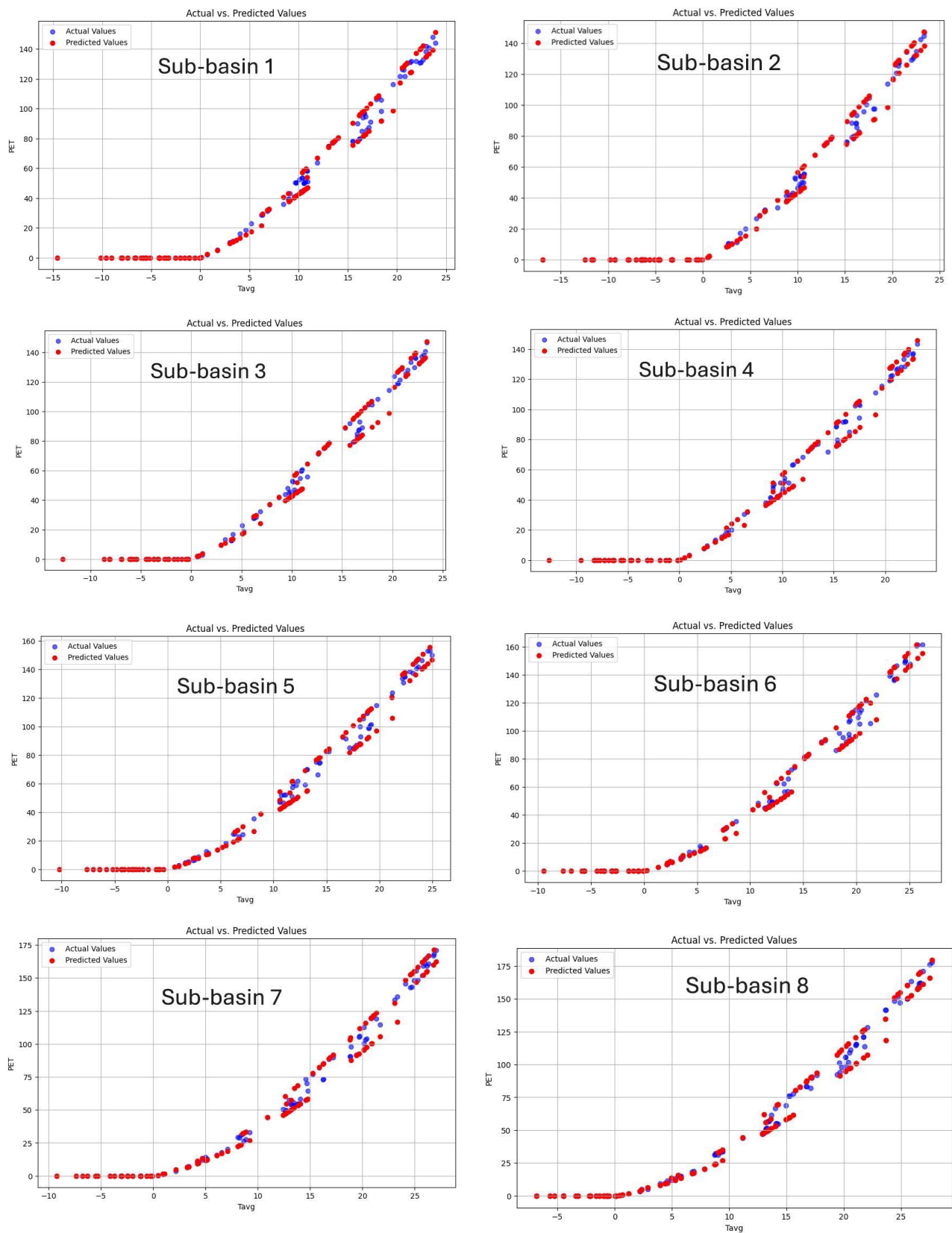


Figure 8. Cont.

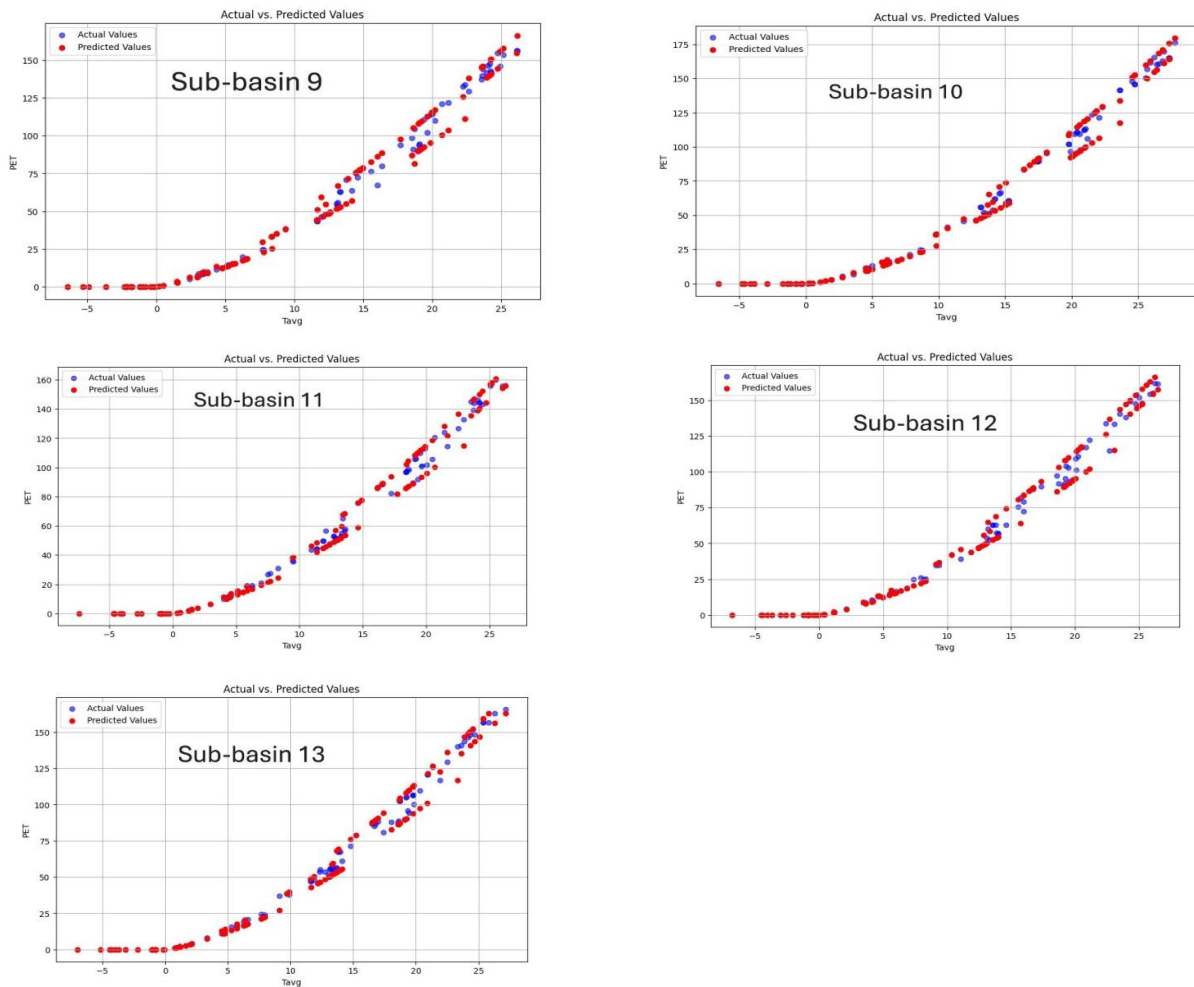


Figure 8. Actual and predicted PET via RF.

The results indicate the model performs well across most sub-basins, as seen in the scatter plots, which reveal a positive correlation between observed and predicted values. In many sub-basins, this relationship is particularly strong, highlighting the model's capability to capture overall patterns in PET. In some scatter plots, deviations from the ideal line indicate chance inaccuracies, which are commonly assumed the complexity of real-world processes. However, the visualization reveals that the model offers a valuable estimate of PET, offering insights that could be applied in water resource management and ecological research. To further quantify and analyze model performance, metrics such as R^2 , RMSE, and MAE should be incorporated. Additionally, conducting a feature importance analysis and addressing the higher-range deviations could enhance the model's reliability and provide insights for improved performance in specific sub-basins.

4.5. Performance of the Models

Table 3 provides a comprehensive assessment of the performance of three algorithms CNN, SVM, and RF in expecting PET results across 13 sub-basins based on average temperature. Three statistical metrics have been used for assessing the results of the proposed models including R^2 , MSE, and RMSE. Below is a detailed analysis of each metric.

Table 3. CNN, SVM, and RF algorithm results.

Algorithms	Sub-Basin 1	Sub-Basin 2	Sub-Basin 3	Sub-Basin 4	Sub-Basin 5	Sub-Basin 6	Sub-Basin 7	Sub-Basin 8	Sub-Basin 9	Sub-Basin 10	Sub-Basin 11	Sub-Basin 12	Sub-Basin 13
R2	CNN	0.962	0.987	0.987	0.987	0.962	0.975	0.987	0.975	0.984	0.986	0.986	0.985
	SVM	0.954	0.954	0.956	0.956	0.953	0.950	0.945	0.945	0.954	0.945	0.953	0.948
	RF	1.000	1.000	1.000	1.000	1.000	1.000	1.000	1.000	1.000	1.000	1.000	1.000
MSE	CNN	0.293	0.287	0.309	0.277	0.345	0.353	0.405	0.422	0.408	0.400	0.377	0.387
	SVM	0.375	0.348	0.287	0.267	0.484	0.661	0.981	1.028	0.548	1.013	0.527	0.680
	RF	0.409	0.326	0.389	0.338	0.439	0.407	0.485	0.640	0.605	0.412	0.331	0.385
RMSE	CNN	0.541	0.536	0.556	0.526	0.587	0.594	0.637	0.649	0.639	0.632	0.614	0.622
	SVM	0.612	0.590	0.536	0.517	0.696	0.813	0.990	1.014	0.740	1.006	0.726	0.825
	RF	0.640	0.571	0.624	0.582	0.663	0.638	0.696	0.800	0.778	0.642	0.575	0.621

Among the models, RF consistently reveals superior performance, attaining the highest R^2 values (1.000) across all sub-basins. These findings indicate that RF effectively captures the relationship between the predictor (average temperature) and target variables (PET) with perfect accuracy. While MSE and RMSE values varied slightly among the sub-basins, they offer additional insights into the model's predictive precision. Moreover, RF accomplishes the lowest MSE and RMSE values in all sub-basins, with a mostly strong performance in Sub-basin 2 (MSE = 0.326, RMSE = 0.571) and Sub-basin 13 (MSE = 0.385, RMSE = 0.621). Conversely, Sub-basin 8 exhibited the highest MSE (0.640) and RMSE (0.649), reflecting relatively larger prediction errors. These results advocate greater prediction challenges in these areas, possibly due to increased data inconsistency or more complex underlying patterns. Despite these differences, the RMSE values across all sub-basins remained consistently low, further validating the model's effectiveness in minimizing errors. These findings underscore RF's capacity to moderate prediction errors and establish it as the most vigorous model for this dataset. The RF model's consistently high accuracy, combined with low MSE and RMSE values, highlights its robustness and reliability in predicting PET across diverse sub-regions, which is in line with previous studies [32,33]. This exceptional performance can be attributed to the model's ability to manage complex datasets effectively and mitigate overfitting through its ensemble learning approach. By combining multiple decision trees, the RF model enhances predictive accuracy and generalization, making it an ideal tool for precise PET estimation across varying climatic and topographic conditions [15].

The CNN model also exhibits strong predictive capabilities, with R^2 values spanning from 0.962 to 0.987. Its best performance is observed in Sub-basin 5, where it attains an MSE of 0.277 and an RMSE of 0.526, reflecting high accuracy. Notable results are also observed in Sub-basin 3 ($R^2 = 0.987$, MSE = 0.309, RMSE = 0.556) and Sub-basin 9 ($R^2 = 0.987$, MSE = 0.405, RMSE = 0.637). However, CNN consistently records slightly higher errors compared to RF across most sub-basins, suggesting it is less effective overall. Despite this, CNN remains a reliable model, though its computational intensity relative to RF may pose practical challenges depending on the application.

In contrast, the SVM algorithm shows mixed performance, with notable weaknesses in certain sub-basins. While its R^2 values are relatively stable and dependable, ranging from 0.945 to 0.956, it exhibits higher error rates in several regions. For example, in Sub-basins 7 and 9, SVM struggles with high MSE values of 0.981 and 1.013 and corresponding RMSE values of 0.990 and 1.014, indicating reduced predictive reliability in areas with greater data complexity or climate variability. However, SVM performs relatively well in Sub-basins 5 and 3, attaining lower error rates (MSE = 0.267 and 0.287, respectively). Despite these strengths, SVM's overall performance is weaker than both RF and CNN, limiting its suitability for this application.

In general, random forest emerges as the most effective and outperforms other models and dependable algorithms, achieving exceptional accuracy and minimal prediction errors

across all sub-basins [32]. CNN offers a viable alternative with consistent and strong performance, particularly in Sub-basins 5 and 3, though it slightly lags behind RF. On the other hand, SVM demonstrates the weakest overall performance, with notable challenges in Sub-basins 7 and 9, suggesting it is less appropriate for this dataset. These results emphasize the robustness of RF in handling data variability, making it the preferred choice for this predictive task.

5. Conclusions

This study delivers an inclusive assessment of machine learning and deep learning models including support vector machine (SVM), convolutional neural network (CNN), and random forest (RF) for predicting PET in the Murat River Basin. Using forty years of monthly temperature data and the temperature-based Thornthwaite equation, this research effectively tackles the challenge of PET prediction in regions with limited data accessibility by integrating advanced computational methods.

The findings indicate that the RF model outperformed other models, achieving a perfect R^2 value of 1.000 across all sub-basins, along with the lowest MSE and RMSE values. This excellent performance is attributed to the RF model's ability to manage complex datasets, reduce overfitting, and accurately capture nonlinear relationships. CNN also established strong predictive accuracy, leveraging its deep learning architecture to recognize complicated patterns within the dataset. While SVM provided reliable predictions, its performance was more sensitive to data quality and hyperparameter differences, making it most operative in sub-basins with simpler or more linear relationships. The spatial and temporal investigation of PET trends exposed notable seasonal fluctuations, with PET values peaking in the summer months and showing a strong positive correlation with increasing temperatures. These results highlight the essential role of temperature in driving evapotranspiration processes, particularly in semi-arid regions where effective water management is critical for ensuring agricultural sustainability. Integrating GIS spatial modeling additionally improved PET prediction accuracy by accounting for variations in topography and climate across the basin. This study underscores the potential of artificial intelligence-driven models to enhance PET estimations, offering valuable contributions to hydrological modeling, water resource management, and agricultural planning in the face of climate change. The RF model, acknowledged as the most robust and accurate, offers a transferable methodology that can be adapted to other regions with similar data limitations. Future research would aim to integrate extra climatic parameters, improve model standardization techniques, and explore collaborative modeling methods to further improve prediction accuracy and generalizability.

By advancing PET prediction methodologies, this research significantly contributes to hydrological science, addressing the pressing need for data-efficient and accurate modeling approaches to meet the challenges posed by climate variability and growing water demand.

To enhance the accuracy and robustness of PET predictions, it is recommended to incorporate additional environmental parameters, such as relative humidity, wind speed, solar radiation, and atmospheric pressure. These factors have been demonstrated to significantly influence PET dynamics, and their inclusion could offer a more comprehensive understanding of the underlying processes. Future research should investigate the potential interactions among these parameters, alongside the existing variables, to refine predictive models and improve their applicability across diverse geographical regions and climate conditions.

Supplementary Materials: The following supporting information can be downloaded at: <https://www.mdpi.com/article/10.3390/su162411077/s1>, Table S1. VPET Results of Thornthwaite Equation for Murad River Basin.

Author Contributions: I.A.H.: Conceptualization, methodology, formal analysis, software, investigation, writing—original draft preparation, visualization. M.I.Y.: validation, formal analysis, data curation, writing—review and editing, supervision, project administration. All authors have read and agreed to the published version of the manuscript.

Funding: This research received no external funding.

Institutional Review Board Statement: Not applicable.

Informed Consent Statement: Informed consent was obtained from all subjects involved in the study.

Data Availability Statement: The data used in this research are reliable data, the climate and meteorological data are available in DSI and EIE it can be founded online or from meteorological directories in Turkey while the geographical data which is DEM were downloaded from USGS.

Acknowledgments: The authors extend their sincere appreciation to the U.S. Geological Survey (USGS) Agency for providing relevant data. Special thanks are also given to the Irrigation Directorate of Erbil for their support during working on this research. Also, the authors express their gratitude to the anonymous reviewers and the editorial team for their insightful suggestions, which have significantly enhanced the quality of this paper.

Conflicts of Interest: The authors declare that they have no known competing financial interests or personal relationships that could have influenced the work reported in this paper.

References

- Wood, E.F.; Su, H.; McCabe, M.; Su, B. Estimating evaporation from satellite remote sensing. In Proceedings of the 2003 IEEE International Geoscience and Remote Sensing Symposium, IGARSS 2003, Toulouse, France, 21–25 July 2003; Proceedings (IEEE Cat. No. 03CH37477). IEEE: Piscataway, NJ, USA, 2003.
- Jing, W.; Yaseen, Z.M.; Shahid, S.; Saggi, M.K.; Tao, H.; Kisi, O.; Salih, S.Q.; Al-Ansari, N.; Chau, K.-W. Implementation of evolutionary computing models for reference evapotranspiration modeling: Short review, assessment, and possible future research directions. *Eng. Appl. Comput. Fluid Mech.* **2019**, *13*, 811–823. [\[CrossRef\]](#)
- Raman, J.; Kim, J.-S.; Choi, K.R.; Eun, H.; Yang, D.; Ko, Y.-J.; Kim, S.-J. Application of lactic acid bacteria (LAB) in sustainable agriculture: Advantages and limitations. *Int. J. Mol. Sci.* **2022**, *23*, 7784. [\[CrossRef\]](#)
- Pelosi, A.; Villani, P.; Bolognesi, S.F.; Chirico, G.B.; D’urso, G. Predicting crop evapotranspiration by integrating ground and remote sensors with air temperature forecasts. *Sensors* **2020**, *20*, 1740. [\[CrossRef\]](#)
- Penman, H.L. Natural evaporation from open water, bare soil, and grass. *Proc. R. Soc. Lond. Ser. A Math. Phys. Sci.* **1948**, *193*, 120–145.
- Shuttleworth, W. *Evaporation Handbook of Hydrology ed DR Maidment*; McGraw-Hill: New York, NY, USA, 1993.
- Allen, R.G.; Clemmens, A.J.; Burt, C.M.; Solomon, K.; O’Halloran, T. Prediction accuracy for projectwide evapotranspiration using crop coefficients and reference evapotranspiration. *J. Irrig. Drain. Eng.* **2005**, *131*, 24–36. [\[CrossRef\]](#)
- Aschonitis, V.; Touloumidis, D.; ten Veldhuis, M.-C.; Coenders-Gerrits, M. Correcting Thornthwaite potential evapotranspiration using a global grid of local coefficients to support temperature-based estimations of reference evapotranspiration and aridity indices. *Earth Syst. Sci. Data* **2022**, *14*, 163–177. [\[CrossRef\]](#)
- Brutsaert, W. Global land surface evaporation trend during the past half-century: Corroboration by Clausius-Clapeyron scaling. *Adv. Water Resour.* **2017**, *106*, 3–5. [\[CrossRef\]](#)
- Bouchet, R. Evapotranspiration réelle, evapotranspiration potentielle, et production agricole. *Ann. Agron.* **1963**, *14*, 743–824.
- Thornthwaite, C.W. An approach toward a rational classification of climate. *Geogr. Rev.* **1948**, *38*, 55–94. [\[CrossRef\]](#)
- Ahmadi, F.; Mehdizadeh, S.; Mohammadi, B.; Pham, Q.B.; Doan TN, C.; Vo, N.D. Application of an artificial intelligence technique enhanced with intelligent water drops for monthly reference evapotranspiration estimation. *Agric. Water Manag.* **2021**, *244*, 106622. [\[CrossRef\]](#)
- Fahimi, F.; Yaseen, Z.M.; El-Shafie, A. Application of soft computing based hybrid models in hydrological variables modeling: A comprehensive review. *Theor. Appl. Climatol.* **2017**, *128*, 875–903. [\[CrossRef\]](#)
- Mehr, A.D.; Nourani, V.; Kahya, E.; Hrnjica, B.; Sattar, A.M.; Yaseen, Z.M. Genetic programming in water resources engineering: A state-of-the-art review. *J. Hydrol.* **2018**, *566*, 643–667. [\[CrossRef\]](#)
- Shahbazi, A.N.; Zahraie, B.; Nasser, M. Seasonal meteorological drought prediction using support vector machine. *World Appl. Sci. J.* **2012**, *13*, 1387–1397.
- Chen, Z.; Sun, S.; Wang, Y.; Wang, Q.; Zhang, X. Temporal convolution-network-based models for modeling maize evapotranspiration under mulched drip irrigation. *Comput. Electron. Agric.* **2020**, *169*, 105206. [\[CrossRef\]](#)
- Hassan, M.A.; Khalil, A.; Kaseb, S.; Kassem, M. Exploring the potential of tree-based ensemble methods in solar radiation modeling. *Appl. Energy* **2017**, *203*, 897–916. [\[CrossRef\]](#)
- Papadopoulos, S.; Azar, E.; Woon, W.-L.; Kontokosta, C.E. Evaluation of tree-based ensemble learning algorithms for building energy performance estimation. *J. Build. Perform. Simul.* **2018**, *11*, 322–332. [\[CrossRef\]](#)

19. Granata, F.; Di Nunno, F. Forecasting evapotranspiration in different climates using ensembles of recurrent neural networks. *Agric. Water Manag.* **2021**, *255*, 107040. [[CrossRef](#)]
20. Deng, L.; Yu, D. Deep learning: Methods and applications. *Found. Trends® Signal Process.* **2014**, *7*, 197–387. [[CrossRef](#)]
21. Fattah, W.H.; IMi, Y. Hydrological analysis of Murat river basin. *Int. J. Appl.* **2015**, *5*, 47–55.
22. Terakawa, A. *Hydrological Data Management: Present State and Trends*; Secretariat of the World Meteorological Organization: Geneva, Switzerland, 2003.
23. Naoum, S.; Tsanis, I. Ranking spatial interpolation techniques using a GIS-based DSS. *Glob. Nest* **2004**, *6*, 1–20.
24. Chai, H.; Cheng, W.; Zhou, C.; Chen, X.; Ma, X.; Zhao, S. Analysis and comparison of spatial interpolation methods for temperature data in Xinjiang Uygur Autonomous Region, China. *Nat. Sci.* **2011**, *3*, 999. [[CrossRef](#)]
25. Anggraini, N.; Slamet, B. Thornthwaite Models for Estimating Potential Evapotranspiration in Medan City. *IOP Conf. Ser. Earth Environ. Sci.* **2021**, *912*, 012095. [[CrossRef](#)]
26. Azman, R.; Noor, N.; Abdullah, S.; Ideris, M. Analysis of Drought Index in Sub-Urban Area Using Standard Precipitation Evapotranspiration Index (SPEI). *Int. J. Integr. Eng.* **2022**, *14*, 157–163. [[CrossRef](#)]
27. Kim, S.-J.; Bae, S.-J.; Jang, M.-W. Linear regression machine learning algorithms for estimating reference evapotranspiration using limited climate data. *Sustainability* **2022**, *14*, 11674. [[CrossRef](#)]
28. Pramanik, M.; Chowdhury, K.; Rana, M.J.; Bisht, P.; Pal, R.; Szabo, S.; Pal, I.; Behera, B.; Liang, Q.; Padmadas, S.S.; et al. Climatic influence on the magnitude of COVID-19 outbreak: A stochastic model-based global analysis. *Int. J. Environ. Health Res.* **2022**, *32*, 1095–1110. [[CrossRef](#)] [[PubMed](#)]
29. Wang, Q.; Ma, Y.; Zhao, K.; Tian, Y. A Comprehensive Survey of Loss Functions in Machine Learning. *Ann. Data Sci.* **2022**, *9*, 187–212. [[CrossRef](#)]
30. Tian, Y.; Su, D.; Lauria, S.; Liu, X. Recent advances in loss functions in deep learning for computer vision. *Neurocomputing* **2022**, *497*, 129–158. [[CrossRef](#)]
31. Paul, S.; Farzana, S.Z.; Das, S.; Das, P.; Kashem, A. Comparative analysis of advanced deep learning models for predicting evapotranspiration based on meteorological data in bangladesh. *Environ. Sci. Pollut. Res.* **2024**, *31*, 60041–60064. [[CrossRef](#)] [[PubMed](#)]
32. Amani, S.; Shafizadeh-Moghadam, H. A review of machine learning models and influential factors for estimating evapotranspiration using remote sensing and ground-based data. *Agric. Water Manag.* **2023**, *284*, 108324. [[CrossRef](#)]
33. Lee, J.K.; Rouault, M.; Wyart, V. Adaptive tuning of human learning and choice variability to unexpected uncertainty. *Sci. Adv.* **2023**, *9*, eadd0501. [[CrossRef](#)] [[PubMed](#)]
34. Liu, S.; Zhou, D.J. Using cross-validation methods to select time series models: Promises and pitfalls. *Br. J. Math. Stat. Psychol.* **2024**, *77*, 337–355. [[CrossRef](#)] [[PubMed](#)]
35. Siva, G. Matrix variate receiver operating characteristic curve for binary classification. *Statistics* **2024**, *58*, 1–8. [[CrossRef](#)]
36. Breiman, L. Random forests. *Mach. Learn.* **2001**, *45*, 5–32. [[CrossRef](#)]
37. Lazar, J.; Feng, J.H.; Hochheiser, H. *Research Methods in Human-Computer Interaction*; Morgan Kaufmann: Burlington, MA, USA, 2017.
38. Feng, F.; Tuomi, M.; Jones, H.R.; Barnes, J.; Anglada-Escude, G.; Vogt, S.S.; Butler, R.P. Color difference makes a difference: Four planet candidates around τ ceti. *Astron. J.* **2017**, *154*, 135. [[CrossRef](#)]
39. Yaseen, Z.M.; Al-Juboori, A.M.; Beyaztas, U.; Al-Ansari, N.; Chau, K.-W.; Qi, C.; Ali, M.; Salih, S.Q.; Shahid, S. Prediction of evaporation in arid and semi-arid regions: A comparative study using different machine learning models. *Eng. Appl. Comput. Fluid Mech.* **2020**, *14*, 70–89. [[CrossRef](#)]
40. Lee, Y.C.; Christensen, J.J.; Parnell, L.D.; Smith, C.E.; Shao, J.; McKeown, N.M.; Ordovás, J.M.; Lai, C.Q. Using Machine Learning to Predict Obesity Based on Genome-Wide and Epigenome-Wide Gene–Gene and Gene–Diet Interactions. *Front. Genet.* **2022**, *12*, 783845. [[CrossRef](#)]
41. Wald, N.J.; Bestwick, J.P. Is the area under an ROC curve a valid measure of the performance of a screening or diagnostic test? *J. Med. Screen.* **2014**, *21*, 51–56. [[CrossRef](#)] [[PubMed](#)]

Disclaimer/Publisher’s Note: The statements, opinions and data contained in all publications are solely those of the individual author(s) and contributor(s) and not of MDPI and/or the editor(s). MDPI and/or the editor(s) disclaim responsibility for any injury to people or property resulting from any ideas, methods, instructions or products referred to in the content.